FRONTIERS OF PHYSICS

RESEARCH ARTICLE
Volume 18 / Issue 3 / 31304 / 2023

Criticality-based quantum metrology in the presence of decoherence

Wan-Ting He, Cong-Wei Lu, Yi-Xuan Yao, Hai-Yuan Zhu, Qing Ai†

Department of Physics, Applied Optics Beijing Area Major Laboratory,
Beijing Normal University, Beijing 100875, China
Corresponding author. E-mail: †aiqing@bnu.edu.cn

Received January 10, 2023; accepted March 7, 2023

ABSTRACT

Because quantum critical systems are very sensitive to the variation of parameters around the quantum phase transition (QPT), quantum criticality has been presented as an efficient resource for metrology. In this paper, we address the issue whether the divergent feature of the inverted variance is realizable in the presence of noise when approaching the QPT. Taking the quantum Rabi model (QRM) as an example, we obtain the analytical result for the inverted variance with single-photon relaxation. We show that the inverted variance may be convergent in time due to the noise. Since the precision of the metrology is very sensitive to the noise, as a remedy, we propose squeezing the initial state to improve the precision under decoherence. In addition, we also investigate the criticality-based metrology under the influence of the two-photon relaxation. Strikingly, although the maximum inverted variance still manifests a power-law dependence on the energy gap, the exponent is positive and depends on the dimensionless coupling strength. This observation implies that the criticality may not enhance but weaken the precision in the presence of two-photon relaxation, due to the non-linearity introduced by the two-photon relaxation.

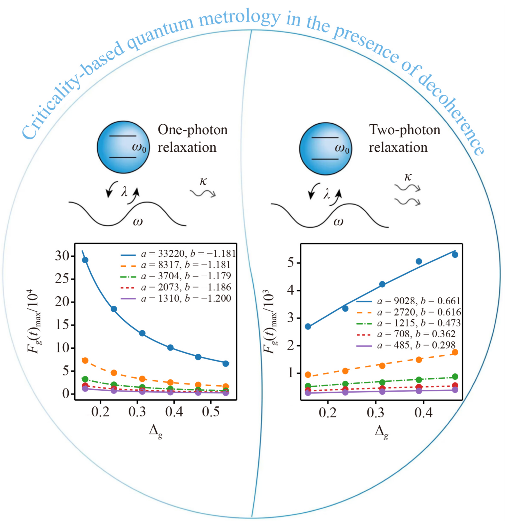

Keywords criticality, quantum, metrology, decoherence

1 Introduction

Quantum criticality has been shown to provide significant advantages for quantum sensing and metrology [1–11]. In quantum phase transition (QPT), a small variation in the order parameter may cause a huge change in the system's properties when approaching the quantum critical point [12–14]. Thus, quantum criticality can be viewed as a valuable resource to acquire an ultrahigh-precision estimation. In the last few years, criticality-based quantum metrological schemes have gained increasing attention among both theoretical and experimental researchers. Many criticality-based quantum metrology protocols in QPT systems have been proposed, which can be classified into two types [4, 5]. One of them focuses on the critical behaviors of the QPT at equilibrium, and utilizes the ground state of the Hamiltonian near the critical point. Unfortunately, it is very inefficient to prepare the ground-state around the critical point by the state-of-art technology. The other focuses on the dynamical behaviors, which evolve under a Hamiltonian close to the critical point. It is quite similar to the interferometric paradigm in the typical quantum metrology. Previous work [3] has revealed that both two kinds of approaches yield the same scaling for a broad class of quantum many-body systems. Recently, a dynamic framework for criticality-

Higher Education Press

arXiv: 2209.10731
https://doi.org/10.1007/s11467-023-1278-2

based quantum metrology, which preliminarily focuses on the dynamical approach, has been proposed [2, 15, 16]. The fundamental idea as well as the details of experimental implementation using quantum Rabi model (QRM) have been illustrated. The QRM is one of the most fundamental models describing quantum light-matter interactions [17]. Ultrastrong light-matter interactions may give rise to a superradiant QPT in the QRM [5, 18–27]. The thermodynamic limit can be achieved when the reduced Rabi frequency approaches infinity in some quantum systems with criticality, such as the Dicke model, the Lipkin–Meshkov–Glick model and the QRM [5].

On the other hand, any quantum system inevitably suffers from the interaction with the surrounding environment and thus forms an open quantum system [28]. Quantum metrology makes use of quantum techniques such as entanglement and squeezing to improve measurement accuracy [29–33]. It has been known over two decades that the quantum metrology with the maximum-entangled states shows no advantage over the classical counterpart when the decoherence is present [29]. Interestingly, when placed in a non-Markovian environment, the entangled probes indeed manifest their superiority by the quantum Zeno effect [30, 34–38], and recently it was experimentally demonstrated by an exact and efficient quantum simulation approach [39–45].

In this work, inspired by the above discoveries, we analyze the achievable precision in the QRM when considering the thermal relaxation. The upper bound on the achievable precision of the metrology will be dramatically reduced owing to the noise. This result indicates that the dissipation poses severe limitations and thus hinders the metrological advantages in this framework. Furthermore, we find that the inverted variance may converge in time no matter as a result of the noise. We further explore optimization of initial state and find that the precision can be improved by a squeezing operation on the initial state. On the other hand, recently two-photon relaxation has been experimentally realized [46]. It was theoretically shown that the two-photon relaxation preserves the Z_2 symmetry of the QRM. The initial states with even–odd parity manifest qualitatively distinct transient and steady state behaviors, which is present both at ultrastrong and weak couplings [47]. It is interesting to consider the two-photon relaxation's impact, which has never been considered on the criticality-based quantum metrology in the QRM. Motivated by these observations, we theoretically investigate the quantum dynamics of the metrology in the presence of two-photon relaxation.

This paper is organized as follows. In Section 2, we outline some basic concepts in the quantum metrology based on the criticality and introduce the QRM with noise. In Section 3, we analyze the results by the semi-classical equation of motion and discuss the effects of various physical parameters on the measurement precision. In Section 4, we investigate the effects of the two-photon relaxation on the metrology. The main conclusions of this paper are drawn in Section 5.

2 Model

In this paper, we consider the QRM for criticality-based quantum metrology, which consists of a two-level system coupled to a single cavity mode. It is the most simplified version of the Dicke model [48]. The Hamiltonian of the QRM is

$$H_{\mathrm{Rabi}} = \omega a^\dagger a + \frac{\omega_0}{2}\sigma_z - \lambda(a + a^\dagger)\sigma_x, \tag{1}$$

where ω is the frequency of the bosonic field, $a^\dagger$ and a are the creation and annihilation operators of the field, ω_0 is the transition frequency of the two-level atom, σ_α ($\alpha = x, y, z$) are the Pauli operators of the atom, λ is the coupling strength. Let $g = 2\lambda/\sqrt{\omega\omega_0}$ be the dimensionless coupling constant. When the ratio of two transition frequencies diverges, i.e., $\eta = \omega_0/\omega \to \infty$, the energy gap closes and there exhibits a second-order normal-to-superradiant QPT at the critical point $g = 1$ [18]. In the limit of $\eta \to \infty$, through the Schrieffer–Wolff transformation $U_{\mathrm{np}} = \exp[g\sqrt{\eta^{-1}}(a + a^\dagger)(\sigma_+ - \sigma_-)/2]$ [49], we can obtain an effective low-energy normal-phase Hamiltonian in the spin-down subspace as [2]

$$H_{\mathrm{np}} = \omega[P^2 + (1 - g^2)X^2]/2, \tag{2}$$

where $X = (a + a^\dagger)/\sqrt{2}$ and $P = \mathrm{i}(a^\dagger - a)/\sqrt{2}$ are the quadrature operators. Let $H_0 = \omega P^2/2$ and $H_1 = \omega X^2/2$. In the limit of $\eta \to \infty$, the transition frequency of the atom is much larger than the frequency of the bosonic field. Thus, the QRM is in the large detuning regime. In this case, there is no transition between the spin states of the atom and the coupling between the atom and the field exerts an effective potential on the bosonic field. Owing to the divergence of Δ^{-1} at the critical point the quantum Fisher information (QFI) for the estimation of the parameter g around the critical point can be expressed as [2]

$$\mathcal{F}_g \simeq 16g^2\frac{\left[\sin(\sqrt{\Delta_g}\omega t) - \sqrt{\Delta_g}\omega t\right]^2}{\Delta_g^3}\mathrm{Var}(P^2)_{|\psi\rangle}, \tag{3}$$

where $\Delta_g = 4(1 - g^2)$ characterizes the energy gap, $\mathrm{Var}(P^2)_{|\psi\rangle} = \langle\psi|P^2|\psi\rangle - \langle\psi|P|\psi\rangle^2$ is the variance of the momentum in the state $|\psi\rangle$. In experiments, the precision of measurement is characterized by the inverted variance as $F_g = \chi_g^2/(\Delta X)^2$ with $\chi_g = \partial_g\langle X\rangle$ and $(\Delta X)^2 = \langle X^2\rangle - \langle X\rangle^2$. Here, $\langle X\rangle$ is the expectation of X. Assume an initial state $|\psi(0)\rangle = |\downarrow\rangle \otimes |\psi\rangle_b$ with the spin in the spin-down state $|\downarrow\rangle$ and the bosonic field state $|\psi\rangle_b = (|0\rangle + \mathrm{i}|1\rangle)/\sqrt{2}$, after the Schrieffer-Wolff transformation. The inverted variance will achieve its local maxima $F_g(\tau) = \chi_g^2/(\Delta X)^2|_{t=\tau} = 8g^2\omega^2\Delta_g^{-2}\tau^2$ at $\tau = 2m\pi/(\sqrt{\Delta_g}\omega)$

with $m \in \mathbb{Z}$. Notice that the inverted variance diverges in the long-time limit. The QFI at the same time is $\mathcal{F}_g(\tau) \simeq 16g^2\omega^2\Delta_g^{-2}\tau^2\mathrm{Var}(P^2)_{|\psi\rangle_b}$. The local maximum of the inverted variance $F_g(\tau)$ is of the same order of the QFI $\mathcal{F}_g(\tau)$.

3 Single-photon relaxation

First of all, we consider the QRM with the single-photon relaxation. The inverted variance can be obtained solving the Lindblad-form master equation numerically by using QuTip [50, 51]. In the $\eta \to \infty$ limit, all the corrections which have an order higher than $\eta^{-1/2}$ become zero. Thus, we have

$$U_{\mathrm{np}}^{\dagger} a U_{\mathrm{np}} \approx a, \tag{4}$$

where we have dropped the terms higher than $\eta^{-1/2}$. Upon the projection onto the spin-down subspace, we obtain the effective master equation $\dot{\rho} = -\mathrm{i}[H_{\mathrm{np}}, \rho] + \gamma_a D[a] + \gamma_h D[a^{\dagger}]$, where $D[a] = a\rho a^{\dagger} - a^{\dagger}a\rho/2 - \rho a^{\dagger}a/2$, γ_a is the decay rate, γ_h is the heating rate [52]. Applying a semiclassical equation of motion for the open QRM [53, 54], we have

$$\begin{aligned}
\frac{\mathrm{d}}{\mathrm{d}t}\langle X\rangle &= -\frac{\gamma_a - \gamma_h}{2}\langle X\rangle + \omega\langle P\rangle, \\
\frac{\mathrm{d}}{\mathrm{d}t}\langle P\rangle &= -\frac{\gamma_a - \gamma_h}{2}\langle P\rangle - \frac{\Delta_g\omega}{4}\langle X\rangle, \\
\frac{\mathrm{d}}{\mathrm{d}t}\langle X^2\rangle &= -(\gamma_a - \gamma_h)\langle X^2\rangle + \omega\langle G\rangle + \frac{\gamma_a + \gamma_h}{2}, \\
\frac{\mathrm{d}}{\mathrm{d}t}\langle P^2\rangle &= -(\gamma_a - \gamma_h)\langle P^2\rangle - \frac{\Delta_g\omega}{4}\langle G\rangle + \frac{\gamma_a + \gamma_h}{2}, \\
\frac{\mathrm{d}}{\mathrm{d}t}\langle G\rangle &= -(\gamma_a - \gamma_h)\langle G\rangle + 2\omega\langle P^2\rangle - \frac{\Delta_g\omega}{2}\langle X^2\rangle,
\end{aligned} \tag{5}$$

where $\langle\cdot\rangle = \mathrm{Tr}(\cdot\rho_b)$ with ρ_b being the density matrix of the bosonic field and $G = XP + PX$. In general, $\gamma_a = \kappa(\bar{n}+1)$ and $\gamma_h = \kappa\bar{n}$ describe the coupling of the field to a thermal reservoir at temperature T with mean number

$$\bar{n} = \frac{1}{\mathrm{e}^{\omega/(k_B T)} - 1} \tag{6}$$

of thermal photons, k_B the Boltzmann constant, κ the decay rate at zero temperature [52]. By solving Eq. (5), the inverted variance $F_g(t)$ is analytically given as

$$F_g(t) = \frac{4\Delta_g^{-2}(4-\Delta_g)A^2(t)}{B(t) + \frac{2n+1}{\Delta_g\omega^2+\kappa^2}C(t)}, \tag{7}$$

where the three time-dependent factors are respectively

$$\begin{aligned}
A(t) = {}& [\Delta_g\omega t\langle X(0)\rangle + 4\langle P(0)\rangle]\sin\left(\frac{1}{2}\sqrt{\Delta_g}\omega t\right) \\
& - 2\sqrt{\Delta_g}\omega t\langle P(0)\rangle\cos\left(\frac{1}{2}\sqrt{\Delta_g}\omega t\right),
\end{aligned} \tag{8}$$

$$\begin{aligned}
B(t) = {}& 2\Delta_g[1+\cos(\sqrt{\Delta_g}\omega t)]\mathrm{Var}(X^2)_{|\psi(0)\rangle} \\
& + 8[1-\cos(\sqrt{\Delta_g}\omega t)]\mathrm{Var}(P^2)_{|\psi(0)\rangle} \\
& + 8\sqrt{\Delta_g}\sin(\sqrt{\Delta_g}\omega t)\mathrm{Re}[\mathrm{Cov}(X,P)],
\end{aligned} \tag{9}$$

$$\begin{aligned}
C(t) = {}& \Delta_g(\Delta_g\omega^2 + 4\omega^2 + 2\kappa^2)(\mathrm{e}^{\kappa t} - 1) - (4-\Delta_g) \\
& \times\{\kappa^2[1-\cos(\sqrt{\Delta_g}\omega t)] + \sqrt{\Delta_g}\omega\kappa\sin(\sqrt{\Delta_g}\omega t)\}.
\end{aligned} \tag{10}$$

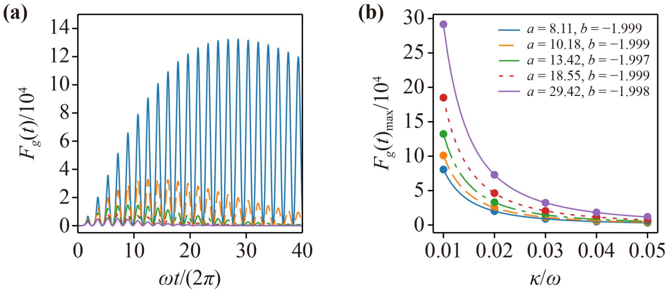

Fig. 1 The effect of the noise strength κ on the precision of the criticality-enhanced metrology. **(a)** The inverted variance of the QRM in the vicinity of the critical point, e.g., $g = 0.96$, when coupling with a thermal reservoir at zero temperature, for $100\kappa/\omega = 1, 2, 3, 4, 5$. They correspond to the blue solid, orange dashed, green dash-dotted, red dotted, purple solid line, respectively. **(b)** The maximum of the inverted variance as a function of the noise parameter κ. From the bottom to the top, the five curves correspond to $g = 0.94, 0.95, 0.96, 0.97, 0.98$, respectively. The dots are obtained from the master equation, while the curves are calculated by the numerical fitting.

Here, $\langle X(0)\rangle$ and $\langle P(0)\rangle$ are the expectation values of the position and momentum operators over the initial state of the bosonic field $|\psi(0)\rangle$, $\mathrm{Cov}(X,P) = \langle\psi(0)|XP|\psi(0)\rangle - \langle\psi(0)|X|\psi(0)\rangle\langle\psi(0)|P|\psi(0)\rangle$. When the noise is absent, i.e., $\kappa = 0$, it can be proven that the local maximum of the inverted variance at the evolution time $\tau = 2m\pi/(\sqrt{\Delta_g}\omega)$ is equal to $16g^2\omega^2\Delta_g^{-2}\tau^2\langle P(0)\rangle^2/(\Delta X(0))^2$ [2]. It scales quadratically with τ, and shows a divergent feature when approaching the critical point, i.e., $F_g(\tau) \propto \Delta_g^{-3} \to \infty$.

At zero temperature, the average photon number $\bar{n}$ equals zero. In this case, we assume the same initial state $(|0\rangle + \mathrm{i}|1\rangle)/\sqrt{2}$ as Ref. [4]. Figure 1 shows the inverted variance of the QRM close to the critical point when coupling with a thermal reservoir at zero temperature. As shown in Fig. 1(a), the dynamics of $F_g(t)$ manifest abundant phenomena. At first, the envelope increases along with the increase of the time. Then, after passing the maximum, it decreases and converges due to the noise. It is in sharp contrast to the prediction when the noise is absent. Furthermore, we also investigate the maximum values of $F_g(t)$ for different κ's in Fig. 1(b). As shown by the numerical fitting, the dependence of the maximum inverted variance $F_g(t)|_{\max}$ on κ can be

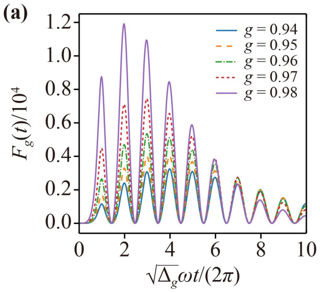

Fig. 2 The effect of the energy gap Δ_g on the precision of the criticality-enhanced metrology. **(a)** The inverted variance F_g of the QRM when approaching the critical point, e.g. $g = 0.94, 0.95, 0.96, 0.97, 0.98$, with the noise parameter $\kappa = 0.05\omega$. It is plotted against the rescaled time $\sqrt{\Delta_g}\omega t/(2\pi)$ to highlight the behavior that in the representation of the rescaled time F_g's oscillate with the same frequency for different g's. **(b)** The maximum of F_g vs. Δ_g for $100\kappa/\omega = 1, 2, 3, 4, 5$, which correspond to the curves from the top to the bottom. The dots are obtained from the master equation, while the curves are calculated by the numerical fitting.

well described by $a\kappa^b$. For different g's, although a's are distinct, all b's are non-exceptionally equal to 2.

In Fig. 2(a), we plot the time dependence of $F_g(t)$ near the critical point for different g's. Notice that the time is rescaled by $\Delta_g\omega/(2\pi)$, which is approximately the oscillating frequency of $F_g(t)$ for small $\kappa \ll \omega$. Similarly as in Fig. 1(a), we can see that $F_g(t)$ gradually increase from their initial values $F_g(0) = 0$ to the maximum values. Then, $F_g(t)$ begins to decrease and eventually vanishes in the long-time limit. By theoretically obtaining $F_g(t)$ under different κ's, we plot the relation of the maximum of $F_g(t)$ with respect to Δ_g in Fig. 2(b). We can see that $F_g(t)$ decays as Δ_g increases for a given κ. It indicates that the noise hinders the metrological advantages in this framework. Again, we numerically fit the maximum of $F_g(t)$ as a function of Δ_g, i.e., $a\Delta_g^b$. Despite of different a's, all curves consistently decays with a nearly-identical $b \simeq -1.18 > -2$, which is the noise-free case. This implies that in the noisy QRM, the inverted variance still diverges when approaching the critical point, i.e., $\Delta_g \to 0$. In other words, by the scaling behavior, we theoretically prove that the criticality-based metrology is robust in the presence of single-photon relaxation.

We now investigate the influence of average photon number. As it can be seen from Fig. 3(a), the time-rescaled $F_g(t)$'s for different g's reach their local maxima at the same period while maximum values of $F_g(t)$ decay as $\bar{n}$ increases. Again, we plot the maximum $F_g(t)$ vs the temperature T in Fig. 3(b). It is shown that the maximum $F_g(t)$ drops dramatically as T rises. This observation reminds us that although the criticality-based metrology seems immune to the noise, the precision is very sensitive to the temperature. Hereafter, we will propose some method to relieve this disadvantage.

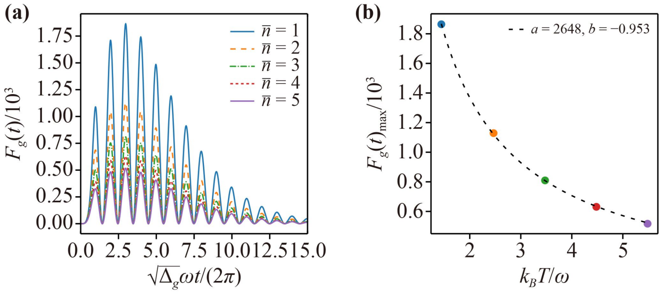

Fig. 3 The effect of the temperature T on the precision of the criticality-enhanced metrology. **(a)** The inverted variance of the QRM close to the critical point, at $g = 0.96$, with $\bar{n} = 1, 2, 3, 4, 5$ and $\kappa/\omega = 0.05$. **(b)** The maximum inverted variance vs. the temperature T. The balck dotted line is numerically fitted by $a(k_BT/\omega)^b$ with $a = 2648$ and $b = -0.953$.

According to Eq. (7), the measurement accuracy highly depends on the initial state. This observation inspires us to perform a squeezing operation, defined by a squeezing operator $S(\xi) = \exp[(\xi^* a^2 - \xi a^{\dagger 2})/2]$, on the initial bosonic field state, where ξ is the squeezing parameter. As seen in Fig. 4, the maximum of $F_g(t)$ is significantly increased as ξ is enlarged. Lines in Fig. 4(b) are numerically fitted by $a\exp(b\xi)$. We further explore the effects of squeezing parameter. We first consider the thermal reservoir at the zero temperature and plot the maxima of F_g vs the squeezing parameter ξ in Fig. 5(a). The numerically-fitted results are similar to Fig. 1(b), with all b's non-exceptionally equal to 2, although a increases along with ξ. This implies that the squeezing operation does not change the scaling behavior. Then, we take the temperature into account. We plot the relation between the maximum of F_g and ξ at different temperatures in Fig. 5(b). We can also observe that the maximum of $F_g(t)$ increases as ξ increases. Although this gain can not completely offset the influence of decoherence, it offers an alternative way to improve the precision under decoherence.

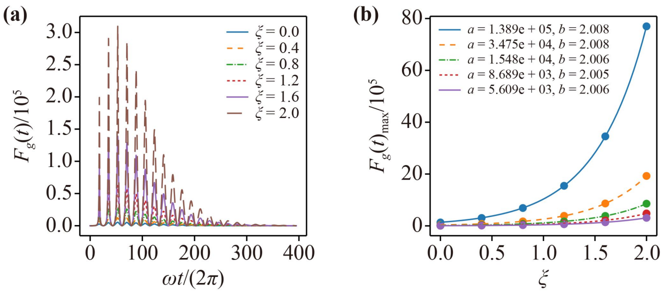

Fig. 4 Improving the precision by performing a squeezing operation on the initial state. **(a)** $F_g(t)$ versus time t, with different squeezing parameter ξ, when $g = 0.96$ and $\kappa/\omega = 0.05$. **(b)** The maximum of F_g at different ξ's with $100\kappa/\omega = 1, 2, 3, 4, 5$.

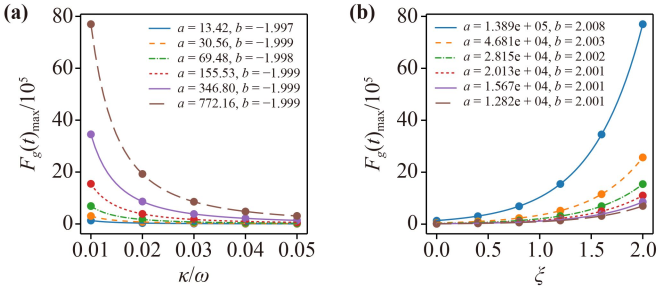

Fig. 5 The effects of the squeezing parameter ξ. **(a)** At zero temperature, the maxima of F_g vs. κ when $g = 0.96$ and $\xi = 0,\ 0.4,\ 0.8,\ 1.2,\ 1.6,\ 2$, which correspond to the curves from the bottom to the top. **(b)** The maximum of F_g at different ξ's for $k_B T/\omega = 0,\ 1,\ 2,\ 3,\ 4,\ 5$, which correspond to the curves from the top to the bottom. The dots are obtained from the master equation, while the curves are calculated by the numerical fitting.

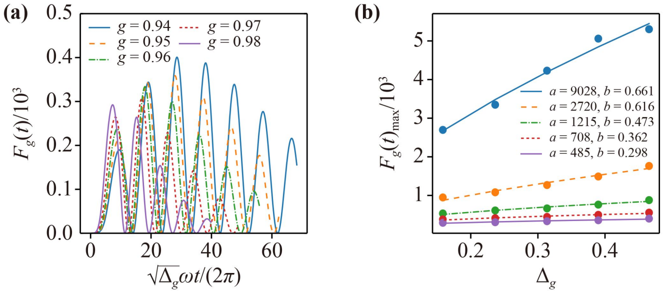

Fig. 6 The effects of the two-photon relaxation. **(a)** The inverted variance F_g of the QRM when approaching the critical point, e.g., $g = 0.94, 0.95, 0.96, 0.97, 0.98$, with the noise parameter $\kappa = 0.05\omega$. It is plotted against the rescaled time $\sqrt{1-g^2}\omega t/\pi$. **(b)** The maximum of F_g at different g's with $100\kappa/\omega = 1,\ 2,\ 3,\ 4,\ 5$. The dots are obtained from the master equation, while the curves are calculated by the numerical fitting.

4 Two-photon relaxation

In the above investigations, we explore the quantum metrology in the presence of single-photon relaxation. However, the quantum dynamics of the QRM with single-photon and two-photon relaxation are totally different [47]. Inspired by this discovery, we study the quantum metrology in the QRM with two-photon relaxation, which can be described by the effective master equation $\dot{\rho} = -\mathrm{i}[H_{\mathrm{np}}, \rho] + \gamma_a D[a^2] + \gamma_h D[a^{\dagger 2}]$ [47].

In Fig. 6(a), we investigate the dynamics of the inverted variance for different g's under the influence of the two-photon relaxation. In contrast to the case with the single-photon relaxation, the quantum dynamics for different g's does not oscillate with the same frequency for the rescaled time. In addition, as g increases, the time to achieve the maximum becomes shorter and shorter. Moreover, we plot the maximum inverted variance as a function of Δ_g in Fig. 6(b). Interestingly, the behavior is quite different from that for the single-photon relaxation in Fig. 1(b). The maximum inverted variance increases monotonically as Δ_g is enlarged. We again numerically fit the data with the function ax^b and thus obtain $a = 9.03 \times 10^3$ and $b = 0.661$ for $\kappa = 0.01\omega$. As κ increases, both a and b reduce dramatically. In other words, when we strengthen the noise, the inverted variance becomes smaller and shows weaker dependence on Δ_g. This remarkable difference can be well described by the Schrödinger equation with a non-Hermitian Hamiltonian H_{tot} [55, 56], in the case of weak relaxation. When there is only single-photon relaxation, the non-Hermitian Hamiltonian H_{tot} is the original Hamiltonian H_{np}, which can be diagonalized by a linear combination of a and $a^{\dagger}$, plus $-\mathrm{i}(\gamma_a a^{\dagger} a + \gamma_h a a^{\dagger})/2$. Although the Hamiltonian H_{tot} is non-Hermitian, the energy spectrum is still equally-spaced, which is fundamentally required by the criticality-based metrology [2]. However, for the case with two-photon relaxation, the non-Hermitian Hamiltonian H_{tot} is the original Hamiltonian H_{np} plus $-\mathrm{i}(\gamma_a a^{\dagger 2} a^2 + \gamma_h a^2 a^{\dagger 2})/2$. Due to the non-linearity introduced by the two-photon relaxation, the energy spectrum is not equally-spaced and thus breaks down the underlying physical mechanism of the criticality-based metrology.

5 Conclusion

We have investigated the impact of decoherence on the criticality-based quantum metrology in the QRM, showing that the achieved precision still diverges when approaching the criticality. In particular, we consider the single-photon relaxation described by the Lindblad-form master equation. By the semiclassical equation of motion, we obtain the analytical solution for the precision characterized by the maximum inverted variance. We have shown that the precision is very sensitive to the temperature. As a remedy, we propose to improve the precision by performing the squeezing operation on the initial state. Furthermore, we also investigate the performance of the metrology in the presence of two-photon relaxation. In contrast to the single-photon relaxation, the inverted variance do not oscillate against the rescaled time at the same frequency for different g's. More strikingly, the maximum inverted variance shows a completely-different tendency when closing to the quantum phase transition.

Acknowledgements This work was supported by Beijing Natural Science Foundation under Grant No. 1202017 and the National Natural Science Foundation of China under Grant Nos. 11674033 and 11505007, and Beijing Normal University under Grant No. 2022129.

References

1. T. L. Heugel, M. Biondi, O. Zilberberg, and R. Chitra, Quantum transducer using a parametric driven-dissipative

phase transition, *Phys. Rev. Lett.* 123(17), 173601 (2019)

2. Y. Chu, S. Zhang, B. Yu, and J. Cai, Dynamic framework for criticality-enhanced quantum sensing, *Phys. Rev. Lett.* 126(1), 010502 (2021)
3. M. M. Rams, P. Sierant, O. Dutta, P. Horodecki, and J. Zakrzewski, At the limits of criticality-based quantum metrology: Apparent super-Heisenberg scaling revisited, *Phys. Rev. X* 8(2), 021022 (2018)
4. L. Garbe, M. Bina, A. Keller, M. G. A. Paris, and S. Felicetti, Critical quantum metrology with a finite-component quantum phase transition, *Phys. Rev. Lett.* 124(12), 120504 (2020)
5. S. Felicetti and A. Le Boité, Universal spectral features of ultrastrongly coupled systems, *Phys. Rev. Lett.* 124(4), 040404 (2020)
6. T. Ilias, D. Yang, S. F. Huelga, and M. B. Plenio, Criticality-enhanced quantum sensing via continuous measurement, *PRX Quantum* 3(1), 010354 (2022)
7. P. Zanardi, M. G. A. Paris, and L. C. Venuti, Quantum criticality as a resource for quantum estimation, *Phys. Rev. A* 78(4), 042105 (2008)
8. M. Tsang, Quantum transition-edge detectors, *Phys. Rev. A* 88(2), 021801 (2013)
9. S. Fernández-Lorenzo and D. Porras, Quantum sensing close to a dissipative phase transition: Symmetry breaking and criticality as metrological resources, *Phys. Rev. A* 96(1), 013817 (2017)
10. K. Gietka, F. Metz, T. Keller, and J. Li, Adiabatic critical quantum metrology cannot reach the Heisenberg limit even when shortcuts to adiabaticity are applied, *Quantum* 5, 489 (2021)
11. X. Y. Lü, W. M. Zhang, S. Ashhab, Y. Wu, and F. Nori, Quantum-criticality-induced strong Kerr nonlinearities in optomechanical systems, *Sci. Rep.* 3(1), 2943 (2013)
12. S. Sachdev, Quantum Phase Transitions, Cambridge University Press, UK, 2011
13. H. T. Quan, Z. Song, X. F. Liu, P. Zanardi, and C. P. Sun, Decay of Loschmidt echo enhanced by quantum criticality, *Phys. Rev. Lett.* 96(14), 140604 (2006)
14. Q. Ai, Y. D. Wang, G. L. Long, and C. P. Sun, Two mode photon bunching effect as witness of quantum criticality in circuit QED, *Sci. China Ser. G* 52(12), 1898 (2009)
15. S. S. Pang and A. N. Jordan, Optimal adaptive control for quantum metrology with time-dependent Hamiltonians, *Nat. Commun.* 8(1), 14695 (2017)
16. S. Pang and T. A. Brun, Quantum metrology for a general Hamiltonian parameter, *Phys. Rev. A* 90(2), 022117 (2014)
17. M. O. Scully and M. S. Zubairy, Quantum Optics, Cambridge University Press, UK, 1997
18. M. J. Hwang, R. Puebla, and M. B. Plenio, Quantum phase transition and universal dynamics in the Rabi model, *Phys. Rev. Lett.* 115(18), 180404 (2015)
19. R. Puebla, M. J. Hwang, J. Casanova, and M. B. Plenio, Probing the dynamics of a superradiant quantum phase transition with a single trapped ion, *Phys. Rev. Lett.* 118(7), 073001 (2017)
20. J. S. Pedernales, I. Lizuain, S. Felicetti, G. Romero, L. Lamata, and E. Solano, Quantum Rabi model with trapped ions, *Sci. Rep.* 5(1), 15472 (2015)
21. D. Lv, S. An, Z. Liu, J. N. Zhang, J. S. Pedernales, L. Lamata, E. Solano, and K. Kim, Quantum simulation of the quantum Rabi model in a trapped ion, *Phys. Rev. X* 8(2), 021027 (2018)
22. A. Frisk Kockum, A. Miranowicz, S. De Liberato, S. Savasta, and F. Nori, Ultrastrong coupling between light and matter, *Nat. Rev. Phys.* 1(1), 19 (2019)
23. W. Salmon, C. Gustin, A. Settineri, O. Di Stefano, D. Zueco, S. Savasta, F. Nori, and S. Hughes, Gauge-independent emission spectra and quantum correlations in the ultrastrong coupling regime of open system cavity-QED, *Nanophotonics* 11(8), 1573 (2022)
24. S. Hughes, A. Settineri, S. Savasta, and F. Nori, Resonant Raman scattering of single molecules under simultaneous strong cavity coupling and ultrastrong optomechanical coupling in plasmonic resonators: Phonon-dressed polaritons, *Phys. Rev. B* 104(4), 045431 (2021)
25. A. Mercurio, V. Macrì, C. Gustin, S. Hughes, S. Savasta, and F. Nori, Regimes of cavity QED under incoherent excitation: From weak to deep strong coupling, *Phys. Rev. Res.* 4(2), 023048 (2022)
26. Y. H. Chen, A. Miranowicz, X. Chen, Y. Xia, and F. Nori, Enhanced-fidelity ultrafast geometric quantum computation using strong classical drives, *Phys. Rev. Appl.* 18(6), 064059 (2022)
27. V. Macrì, A. Mercurio, F. Nori, S. Savasta, and C. Sánchez Muñoz, Spontaneous scattering of Raman photons from cavity-QED systems in the ultrastrong coupling regime, *Phys. Rev. Lett.* 129(27), 273602 (2022)
28. D. J. Zhang and D. M. Tong, Approaching Heisenberg scalable thermometry with built-in robustness against noise, *npj Quantum Inf.* 8, 81 (2022)
29. S. F. Huelga, C. Macchiavello, T. Pellizzari, A. K. Ekert, M. B. Plenio, and J. I. Cirac, Improvement of frequency standards with quantum entanglement, *Phys. Rev. Lett.* 79(20), 3865 (1997)
30. A. W. Chin, S. F. Huelga, and M. B. Plenio, Quantum metrology in non-Markovian environments, *Phys. Rev. Lett.* 109(23), 233601 (2012)
31. J. Ma, X. Wang, C. P. Sun, and F. Nori, Quantum spin squeezing, *Phys. Rep.* 509(2-3), 89 (2011)
32. Z. P. Liu, J. Zhang, Ş. K. Özdemir, B. Peng, H. Jing, X. Y. Lü, C. W. Li, L. Yang, F. Nori, and Y. Liu, Metrology with PT-symmetric cavities: Enhanced sensitivity near the PT-phase transition, *Phys. Rev. Lett.* 117(11), 110802 (2016)
33. K. Xu, Y. R. Zhang, Z. H. Sun, H. Li, P. Song, Z. Xiang, K. Huang, H. Li, Y. H. Shi, C. T. Chen, X. Song, D. Zheng, F. Nori, H. Wang, and H. Fan, Metrological characterization of non-Gaussian entangled states of superconducting qubits, *Phys. Rev. Lett.* 128(15), 150501 (2022)
34. A. G. Kofman, S. Ashhab, and F. Nori, Nonperturbative theory of weak pre- and post-selected measurements, *Phys. Rep.* 520(2), 43 (2012)
35. Y. Matsuzaki, S. C. Benjamin, and J. Fitzsimons, Magnetic field sensing beyond the standard quantum limit under the effect of decoherence, *Phys. Rev. A* 84(1), 012103 (2011)

36. Q. Ai, Y. Li, H. Zheng, and C. P. Sun, Quantum anti-Zeno effect without rotating wave approximation, *Phys. Rev. A* 81(4), 042116 (2010)
37. Q. Ai, D. Xu, S. Yi, A. G. Kofman, C. P. Sun, and F. Nori, Quantum anti-zeno effect without wave function reduction, *Sci. Rep.* 3(1), 1752 (2013)
38. P. M. Harrington, J. T. Monroe, and K. W. Murch, Quantum Zeno effects from measurement controlled qubit-bath interactions, *Phys. Rev. Lett.* 118(24), 240401 (2017)
39. X. Y. Long, W. T. He, N. N. Zhang, K. Tang, Z. D. Lin, H. F. Liu, X. F. Nie, G. R. Feng, J. Li, T. Xin, Q. Ai, and D. W. Lu, Entanglement-enhanced quantum metrology in colored noise by quantum Zeno effect, *Phys. Rev. Lett.* 129(7), 070502 (2022)
40. I. Buluta and F. Nori, Quantum simulators, *Science* 326(5949), 108 (2009)
41. I. M. Georgescu, S. Ashhab, and F. Nori, Quantum simulation, *Rev. Mod. Phys.* 86(1), 153 (2014)
42. N. N. Zhang, M. J. Tao, W. T. He, X. Y. Chen, X. Y. Kong, F. G. Deng, N. Lambert, and Q. Ai, Efficient quantum simulation of open quantum dynamics at various Hamiltonians and spectral densities, *Front. Phys.* 16(5), 51501 (2021)
43. B. X. Wang, M. J. Tao, Q. Ai, T. Xin, N. Lambert, D. Ruan, Y. C. Cheng, F. Nori, F. G. Deng, and G. L. Long, Efficient quantum simulation of photosynthetic light harvesting, *npj Quantum Inf.* 4, 52 (2018)
44. X. Y. Chen, N. N. Zhang, W. T. He, X. Y. Kong, M. J. Tao, F. G. Deng, Q. Ai, and G. L. Long, Global correlation and local information flows in controllable non-Markovian open quantum dynamics, *npj Quantum Inf.* 8, 22 (2022)
45. Y. N. Lu, Y. R. Zhang, G. Q. Liu, F. Nori, H. Fan, and X. Y. Pan, Observing information backflow from controllable non-Markovian multichannels in diamond, *Phys. Rev. Lett.* 124(21), 210502 (2020)
46. Z. Leghtas, S. Touzard, I. M. Pop, A. Kou, B. Vlastakis, A. Petrenko, K. M. Sliwa, A. Narla, S. Shankar, M. J. Hatridge, M. Reagor, L. Frunzio, R. J. Schoelkopf, M. Mirrahimi, and M. H. Devoret, Confining the state of light to a quantum manifold by engineered two-photon loss, *Science* 347(6224), 853 (2015)
47. M. Malekakhlagh and A. W. Rodriguez, Quantum Rabi model with two-photon relaxation, *Phys. Rev. Lett.* 122(4), 043601 (2019)
48. R. H. Dicke, Coherence in spontaneous radiation processes, *Phys. Rev.* 93(1), 99 (1954)
49. J. R. Schrieffer and P. A. Wolff, Relation between the Anderson and Kondo Hamiltonians, *Phys. Rev.* 149(2), 491 (1966)
50. H. P. Breuer and F. Petruccione, The Theory of Open Quantum Systems, New York: Oxford University Press, 2002
51. J. R. Johansson, P. D. Nation, and F. Nori, QuTiP: An open-source python framework for the dynamics of open quantum systems, *Comput. Phys. Commun.* 183(8), 1760 (2012)
52. H. J. Carmichael, An Open Systems Approach to Quantum Optics, Berlin: Spring, 1993
53. C. W. Gardiner and P. Zoller, Quantum Noise: A Handbook of Markovian and Non-Markovian Quantum Stochastic Methods with Applications to Quantum Optics, Berlin: Springer, 2004
54. M. J. Hwang, P. Rabl, and M. B. Plenio, Dissipative phase transition in the open quantum Rabi model, *Phys. Rev. A* 97(1), 013825 (2018)
55. Q. Ai, P. B. Li, W. Qin, J. X. Zhao, C. P. Sun, and F. Nori, The NV netamaterial: Tunable quantum hyperbolic metamaterial using nitrogen vacancy centers in diamond, *Phys. Rev. B* 104(1), 014109 (2021)
56. H. Dong, D. Z. Xu, J. F. Huang, and C. P. Sun, Coherent excitation transfer via the dark-state channel in a bionic system, *Light Sci. Appl.* 1(3), e2 (2012)